

Dynamic scaling of photo-double-ionization to electron impact

Anatoli S. Kheifets 

Research School of Physics, The Australian National University, Canberra ACT 0200, Australia



(Received 24 November 2019; accepted 18 February 2020; published 9 March 2020)

We employ an *ab initio* theory to address several inconsistencies of the empirical scaling of photo-double-ionization (PDI) to electron impact ionization suggested by Samson [Phys. Rev. Lett. **65**, 2861 (1990)]. We do so (i) by isolating the only relevant dipole component of the electron impact ionization and (ii) by replacing the static scaling of Samson, who used an effective cross-section area of the ion remainder, with dynamic scaling using the squared momentum of the photoelectron. The modified scaling is tested in the He $1s^2$ isoelectronic sequence and the combined inner shell $1s$ and valence shell $2p$ PDI of the negative F^- ion [Müller *et al.*, Phys. Rev. Lett. **120**, 133202 (2018)].

DOI: [10.1103/PhysRevA.101.032701](https://doi.org/10.1103/PhysRevA.101.032701)

I. INTRODUCTION

Nonsequential single-photon two-electron ionization (photo-double-ionization, PDI) is an archetypal example of an atomic collision process driven entirely by many-electron correlation. As such, it attracted very considerable attention, in both theoretical and experimental research. A comprehensive review of literature on this process was presented recently by Wehlitz [1]. Basic mechanisms of PDI are now well established. According to McGuire [2], the two main mechanisms of PDI can be identified as the knock-out (KO) and shake-off (SO) processes. Both processes are initialized with a single-photon absorption by one of the target electrons. In the following KO process, the primary photoelectron impacts on the parent ion and knocks out the secondary electron in an ionizing, ($e, 2e$)-like collision.¹ In the KO process, after sudden departure of the primary photoelectron, the ion relaxes and shakes off the secondary electron into the continuum. Contributions of the KO and SO processes to PDI have been studied thoroughly in both the valence and inner shells of atoms (see, e.g., [3–5]). The relative strength of the KO and SO processes depends on the photon energy. Near the PDI threshold, the KO process dominates whereas in the asymptotic region of large photon energies the SO process takes over. It will eventually become the only contributing process in the large-photon-energy limit. The SO is greatly assisted by the ground state correlation whereas the KO is largely insensitive to it.

The KO process is intimately linked to electron impact ionization of the singly ionized parent target. Samson [6] expressed this link as the proportionality relation

$$\frac{\sigma_\gamma^{2+}(\omega)}{\sigma_\gamma^+(\omega) + \sigma_\gamma^{2+}(\omega)} = \frac{1}{\pi r^2} \sigma_e^+(E). \quad (1)$$

¹We use ($e, 2e$) as a proxy term for electron impact ionization. In some literature, it is used solely under coincident detection of both photoelectrons, but we will use this term more generally.

Here σ_γ^+ and σ_γ^{2+} are the single and double photoionization cross sections whereas $\sigma_e^+(E)$ is the electron impact ionization cross section of the singly ionized target by the primary photoelectron at the respective energy. The term in the denominator πr^2 represents the effective ionic cross-section area. Samson [6] argued that “all possible electron correlation processes are embodied in σ_e^+ .” This assertion is, in fact, incorrect as the SO process is left out. Indeed, the shake-off electron is released without any external impact. Samson [6] has also tacitly admitted that “the total angular momentum carried off by the electrons will differ” in PDI and ($e, 2e$). These two points put the validity of Eq. (1) in question.

Kheifets [7,8] tried to restore the validity of Eq. (1) by isolating the only relevant dipole component of the electron impact ionization cross section which would reflect the angular momentum transfer $J = 1$ from the photon to the atom. However, such a dipole scaling was found valid only in a very narrow photon energy range near the PDI threshold. At higher photon energies, $\sigma_{e,J=1}^+(E)$ would fall sharply whereas the PDI ratio would remain essentially flat as it approached its asymptotic limit of large photon energies. This may be related to another implicit assumption behind the empirical scaling (1). It is assumed that the energy is conserved between absorption of the photon and impact of the electron on the ion remainder, i.e., $E = \omega - I_p$. The ionization potential I_p here refers to the neutral atomic target. In reality, PDI can proceed via an infinite number of virtual intermediate states without energy conservation. It should only be conserved between the initial and final states. In addition, various singly ionized atomic states are accessible in such half-on-shell collision processes. Therefore, I_p is not uniquely defined here.

Very recently, a new measurement of PDI on the F^- ion was reported by Müller *et al.* [9]. This PDI process was initiated by the photon absorption in the inner $1s$ shell while the secondary electron was emitted from the valence $2p$ shell. Negative ions are strongly correlated many-electron systems which present researchers with multiple experimental and theoretical challenges [10]. It is for this reason that the work by Müller *et al.* [9] was such a breakthrough. To prove the PDI character of their measurement, the authors applied an

empirical scaling suggested by Pattard [11]:

$$\frac{\sigma_{\gamma}^{2+}}{\sigma_{\gamma}^{+}}(E) = R_{\infty} \frac{E^{\alpha}(E + E_0)^{7/2}}{(E + E_1)^{\alpha+7/2}}. \quad (2)$$

Here α is the Wannier exponent, R_{∞} is the asymptotic double-to-single cross-section ratio, and E_0, E_1 are empirically adjustable constants. The scaling (2) bridges continuously the threshold Wannier behavior and the asymptotic limit of high photon energies. It appeared to represent the F^{-} measurement by Müller *et al.* [9] remarkably well.

Availability of the new set of data prompted us to revisit the original idea of Samson [6] and to adjust Eq. (1) to make it work for the present case. This is achieved by replacing the *static* scaling with the effective ionic cross-section area $1/(\pi r^2)$ to a *dynamic* scaling with the squared primary photoelectron momentum k^2 . In addition, it is the ratio of the double-to-*single* rather than double-to-*total* photoionization cross sections that should be scaled to $(e, 2e)$. In F^{-} , the double-to-single ratio is large, 25% in its maximum, and this substitution makes a significant difference. In the following, we demonstrate that this dynamic scaling is more physically appropriate and it has a much wider range of applicability in various atomic and ionic targets. It also draws a different borderline between the KO and SO processes. Near the PDI threshold, both the dynamic and static scalings become equivalent.

For a demonstration, we consider here two different types of atomic targets. First, we revisit our earlier calculations on two-electron atoms and ions performed with the convergent close-coupling (CCC) method [12]. Second, we consider many-electron targets which are left with a closed valence shell after emission of the primary photoelectron. A new theoretical model is developed to treat such processes which include mixed $1s$ - $2p$ PDI of F^{-} . Both approaches can treat PDI of the Li atom [13], which we use as a crosslink between the two models.

II. THEORETICAL MODEL

We treat electron impact ionization of a closed valence shell target (such as the ‘‘hollow’’ F atom in the $1s2s^22p^6$ configuration) within the random phase approximation with exchange (RPAE). Numerically, the RPAE is implemented with the program suite ATOM [14]. We write the PDI cross section leading to creation of the two photoelectrons labeled 2, 4 and the two holes 0, 3 via an intermediate state containing electron 1 and hole 0 as

$$\begin{aligned} \sigma_{\gamma}^{2+}(\omega) &= C_{\gamma} \sum_{1234} |D_{1234}|^2 \delta(\omega - E_2 - E_4 + E_3 + E_0), \\ D_{1234} &= \sum_L \frac{\langle 0|d|1\rangle \langle 13|V_L|42\rangle}{\omega - E_1 + E_0 + i\delta}. \end{aligned} \quad (3)$$

Here $C_{\gamma} = 4\pi^2\alpha a_0^2\omega$ is the photoionization constant expressed via the fine structure constant α and the Bohr radius a_0 . Here and throughout, we use atomic units with $e = m = \hbar = 1$. The amplitude D_{1234} of such a process is exhibited graphically in the left half of Fig. 1(a) with the straight lines pointing to the right and left to exhibit electrons and holes,

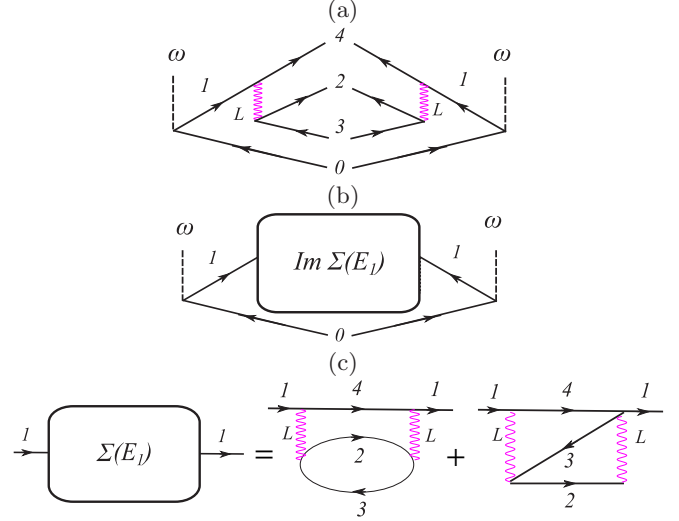


FIG. 1. Graphical representation of PDI in RPAE. (a) The dipole matrix element D_{1234} entering Eq. (4) (left half) and its complex conjugate D_{1234}^* (right half). (b) The squared dipole matrix element $|D_{1234}|^2$ is incorporated into the imaginary self-energy part of the single-electron Green’s function, Eq. (5). (c) Direct and exchange diagrams which represent the irreducible part of the Green’s function. The single-electron Green’s function consists of an infinite sequence of such diagrams (see Figs. 1 and 2 of [15]).

respectively. The dashed lines represent photons whereas the wavy lines stand for the Coulomb interaction. In the right half of this figure we also display the complex conjugate D_{1234}^* as a mirror reflection of D_{1234} and combine their product in Fig. 1(b) into the imaginary self-energy part of the single-electron Green’s function $Im \Sigma(E)$ introduced in [15]. The self-energy defines the correction to the electron scattering phase shift in a formal optical model [16]. We also join the two halves of Fig. 1(a) to conduct an angular momentum projections summation by applying consecutively the graphical summation rule 12.1.2 of Varshalovich *et al.* [17]. As a result, we express the PDI cross-section via the reduced dipole and Coulomb matrix elements as

$$\begin{aligned} \sigma_{\gamma}^{2+}(\omega) &= \frac{1}{3} C_{\gamma} \sum_{1234} \|D_{1234}\|^2 \delta(\omega - E_2 - E_4 + E_3 + E_0), \\ \|D_{1234}\| &= \sum_L \frac{1}{(2L+1)(2l_1+1)} \frac{\langle 0||d||1\rangle \langle 13||V_L||42\rangle}{\omega - E_1 + E_0 + i\delta}. \end{aligned} \quad (4)$$

We adopt the pole approximation $(\omega - E_1 + E_0 + i\delta)^{-1} \simeq -i\pi \delta(\omega - E_1 + E_0)$ and absorb the squared dipole matrix element $\sigma_{01}^+(\omega) = \frac{1}{3} C_{\gamma} |\langle 0||d||1\rangle|^2$ into the single photoionization cross section. Then the PDI cross section is expressed as

$$\begin{aligned} \sigma_{\gamma}^{2+}(\omega) &= \sigma_{\gamma}^+(\omega) (-\pi) Im \Sigma_l(E_1) \\ -\pi Im \Sigma_l(E_1) &= \pi^2 \sum_{234} \sum_L \frac{|\langle 13||V_L||42\rangle|^2}{(2L+1)(2l_1+1)} \\ &\quad \times \delta(E_1 + E_3 - E_2 - E_4) \equiv \mu_{l_1}(E_1) \end{aligned} \quad (5)$$

Here $\mu_l(E)$ is the imaginary part of the phase shift which defines the inelastic electron scattering cross-section [18]

$$\sigma_e^+(E) = \frac{4\pi}{k^2} \sum_J (2J+1) \mu_J(E). \quad (6)$$

Thus the double-to-single cross-section ratio becomes

$$\frac{\sigma_\gamma^{2+}(\omega)}{\sigma_\gamma^+(\omega)} = \mu_{J=1}(E) = \frac{k^2}{12\pi} \sigma_{e,J=1}^+(E). \quad (7)$$

As we have already stressed, the empirical scaling (1) differs from the analytical scaling (7) in two important aspects. First, it is the electron scattering cross section in the dipole channel $J=1$ only that enters Eq. (7). And second, it is the squared photoelectron momentum k^2 rather than the effective ionic cross-section area $1/(\pi r^2)$ that should be taken as the scaling coefficient. The analytical scaling (7) is general whereas the empirical one (1) is target dependent.

A similar scaling can be derived in CCC. We start with the electron scattering cross section given by Eq. (25) of [19] and express it as the spin-weighted average

$$\begin{aligned} \sigma_{e,i \rightarrow f} &= (2\pi)^4 \frac{k_f}{k_i} \frac{1}{4\pi} \sum_{S=0,1} \frac{2S+1}{4} \\ &\times \sum_{L,L',J} \frac{2J+1}{2L_i+1} |\langle n_f l_f L' \| T_{JS} \| n_i l_i L \rangle|^2. \end{aligned} \quad (8)$$

Here the on-shell T matrix is taken between the initial and final two-electron states. For simplicity, we consider the PDI of the He atom in the $1s^2$ ground state and neglect the ground state correlation. In this case, a general expression for the PDI amplitude [20] can be reduced to

$$\begin{aligned} &\langle L k_f n_f l_f \| \mathcal{D} \| 1s^2 \rangle \\ &= \int \! \! \int q^2 dq \frac{\langle L k_f l_f n_f \| T_{JS} \| 1s^+ k_i L' \rangle \langle L' k_i 1s^+ \| d \| 1s^2 \rangle}{E - q^2/2 - \epsilon_f + i0}. \end{aligned} \quad (9)$$

Here $J=1$ and $S=0$ are the total orbital momentum and spin of the electron pair and $E = k_f^2/2 + \epsilon_f$ is the final state energy. We adopt the pole approximation and neglect the principle value integral. We also streamline the notations and write

$$\mathcal{D}_{L_f}(k_f) = -\pi k_i d_{1s}(k_i) \langle L k_f n_f l_f \| T_{JS} \| 1s^+ k_i L' \rangle. \quad (10)$$

The PDI cross section

$$\begin{aligned} \sigma_\gamma^{2+}(k_f) &= C_\gamma \sum_{L_f} \pi k_f |\mathcal{D}_{L_f}(k_f)|^2 = C_\gamma \pi k_i |d_{1s}(k_i)|^2 \\ &\times \left[\pi^2 k_i k_f \sum_{n_f l_f L} |\langle L k_f n_f l_f \| T_{JS} \| 1s^+ k_i L' \rangle|^2 \right] \\ &= \frac{k_i^2}{3\pi} \sigma_\gamma^+(k_i) \sum_{n_f l_f}^{\epsilon_f > 0} \sigma_{e,1s \rightarrow n_f l_f}^+(k_f, k_i). \end{aligned} \quad (11)$$

Here we used the electron scattering cross section (8) in which we isolated the singlet component $S=0$. It is the statistical

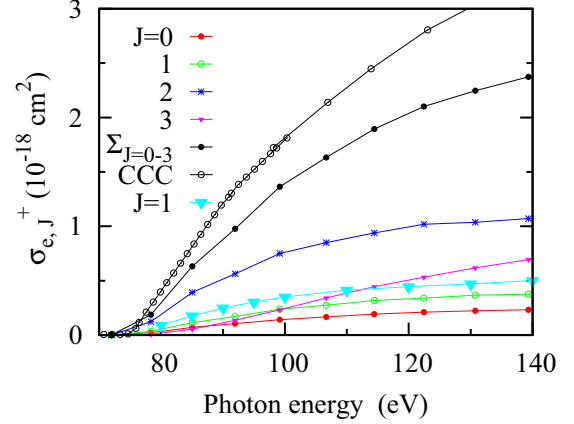


FIG. 2. Electron impact ionization cross section $\sigma_{e,J}^+$ of the Li^+ ion. RPAE calculations with various multiplicities $J=0, 1, 2, 3$ and their sum $\sum_{J=0}^3$ are displayed along with the dipole $J=1$ and total \sum_J CCC calculations from [21].

spin factor $1/4$ that differentiates Eqs. (7) and (11), which otherwise are identical. The occurrence of this factor is related to different representations of the two-electron target in RPAE and CCC. In the former, the ground atomic state is considered as a spin zero $S=0$ “vacuum” with neither holes nor particles present. In the latter, the two particles are always present during the collision process and can be coupled to both the $S=0, 1$ spin states.

III. RESULTS AND DISCUSSION

To ensure compatibility of the CCC and RPAE approaches, we demonstrate that the $(e, 2e)$ process is treated similarly in both models. This test is illustrated graphically in Fig. 2 where we plot various multipole components of the electron impact ionization cross sections $\sigma_{e,J}^+$ on the Li^+ ion in its $1s^2$ ground state. Here we show the RPAE cross sections restricted to various multiplicities $J=0, 1, 2, 3$ and their sum $\sum_{J=0}^3$. We also show the CCC results in the dipole channel $J=1$ and that summed over all the multiplicities \sum_J . The latter result is found to be in perfect agreement with the experiment [21]. Figure 2 shows clearly the difference between the total electron impact ionization cross section and its dipole $J=1$ component, which is only a small fraction of it. So the scalings using empirical expression (1) and the analytical expression (7) must be very different. Second, the dipole components of the RPAE and CCC are quite close, which serves as a test of the compatibility of these two approaches for electron scattering on the closed-shell targets.

Having conducted this test, we proceed with our scaling analysis. First, we analyze our CCC results for PDI of the two-electron He-like targets. In Fig. 3 we show the double-to-single photoionization cross-section ratios $\sigma_\gamma^{2+}/\sigma_\gamma^+$ in He, Li^+ [12], and Mg^{10+} [5] (from top to bottom). In the same figures, we display the respective electron impact ionization cross sections in the dipole channel $\sigma_{e,J=1}^+$ scaled either statically with $(\pi r^2)^{-1}$ or dynamically with k^2 . While both scalings work perfectly well near the threshold, the static scaling goes significantly under the PDI ratio for all targets at

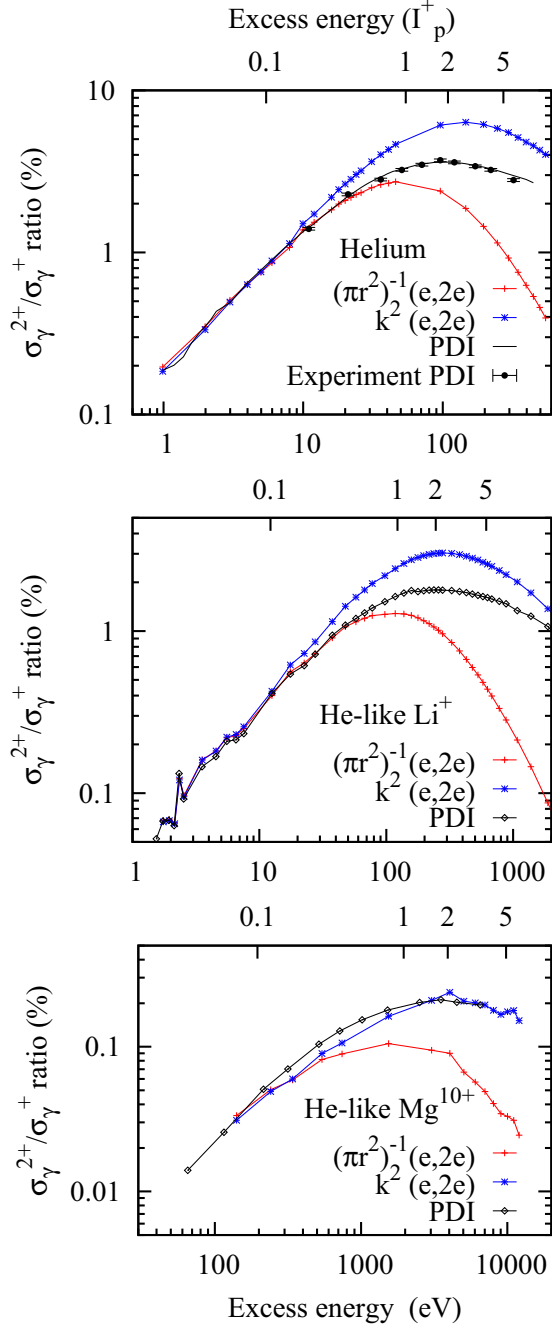


FIG. 3. CCC calculations for the double-to-single $\sigma_{\gamma}^{2+}/\sigma_{\gamma}^{+}$ photoionization cross-section ratios in He, Li^{+} [12], and Mg^{10+} [5] (from top to bottom). The products of σ_e^{+} with $(\pi r^2)^{-1}$ and k^2 are also displayed. The excess energy is shown in eV (bottom axis) and in units of the ionic binding energy I_p^{+} (top axis). Experimental data for PDI of He are from [22]. Numerical values of $\langle r \rangle$ used for scaling theoretical PDI to $(e, 2e)$ are 0.7 (He), 0.47 (Li^{+}), 0.36 (Be^{2+} , not shown), and 0.11 (Mg^{10+}) whereas the corresponding analytical values are 0.75, 0.5, 0.375, and 0.125.

approximately $\sim 0.1I_p^{+}$ away from the threshold. The dynamic scaling, which hinges on the pole approximation, overshoots the PDI ratio at modest excess energies $E \simeq I_p^{+}$ but works progressively better as the ionic charge of the target increases. It becomes nearly perfect for Mg^{10+} up to $10I_p^{+}$.

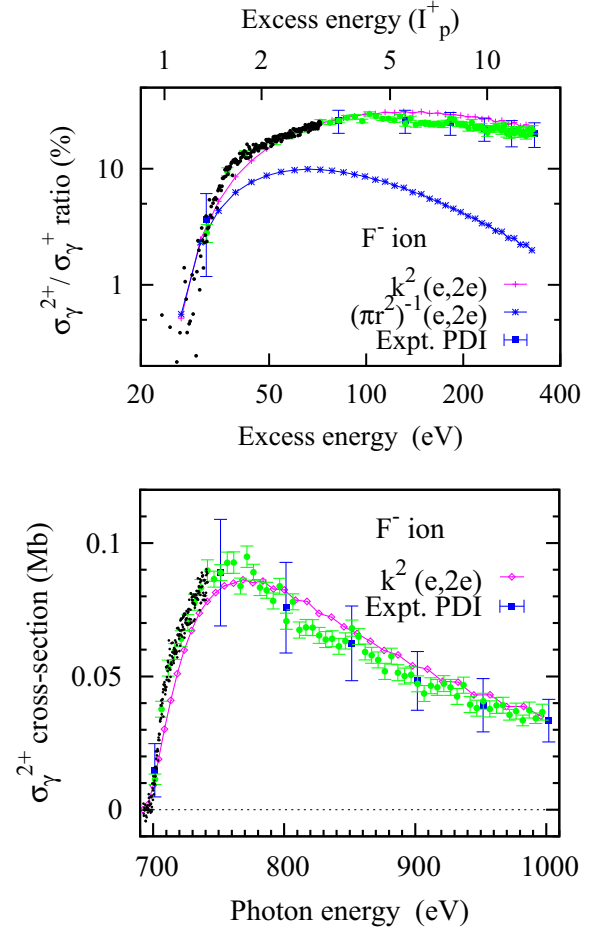


FIG. 4. RPAE calculations for $\sigma_{\gamma}^{2+}/\sigma_{\gamma}^{+}$ photoionization cross-section ratio (top) and PDI cross section σ_{γ}^{2+} (bottom) in the F^{-} ion. Experimental data are displayed with blue absolute error bars, green statistical error bars, and black dots representing a normalized scan as in Fig. 4 of Ref. [9].

It is not coincidental that the static and dynamic scalings merge near the threshold. Indeed, for electron impact ionization of hydrogenic ions that is related to PDI of He-like targets, $\langle r^2 \rangle = 3/Z^2$ and $k^2 = Z^2$ near the threshold. Hence we can transform Eq. (11) into

$$\frac{\sigma_{\gamma}^{2+}}{\sigma_{\gamma}^{+}} = \frac{k^2}{3\pi} \sigma_e^{+} = \frac{1}{\pi \langle r^2 \rangle} \sigma_e^{+}. \quad (12)$$

This is almost identical to Eq. (1) as $\sigma_{\gamma}^{2+} + \sigma_{\gamma}^{+} \approx \sigma_{\gamma}^{+}$ near the PDI threshold where σ_{γ}^{2+} vanishes. Similarly, higher multiplicities of $\sigma_{e, J>1}^{+}$ are suppressed near threshold by the centrifugal barrier, and the dipole cross section can be substituted with the total one.

We continue our scaling analysis in Fig. 4, where we display the double-to-single $\sigma_{\gamma}^{2+}/\sigma_{\gamma}^{+}$ photoionization cross-section ratio (top) and the PDI cross section σ_{γ}^{2+} (bottom) in the F^{-} ion. The single photoionization cross section σ_{γ}^{+} of the K shell of the F atom is taken from [23] and scaled empirically by a factor of 1.4 to match the experiment on F^{-} . Comparison for σ_{γ}^{2+} is made with the experimental data

displayed in Fig. 4 of [13]. We see that the dynamic scaling of the $(e, 2e)$ cross section makes a nearly perfect agreement with the experiment over the whole accessible photon energy range. In the meantime, the static scaling only matches the experimental data near the threshold.

Results displayed in Figs. 3 and 4 are very indicative. The electron impact ionization is indeed the driver of the PDI by the KO process in a fairly wide range of photon energies. The scaling of PDI to $(e, 2e)$ with the k^2 factor is general. The target-dependent $(\pi r^2)^{-1}$ scaling is the special case of the dynamic k^2 scaling which holds near the PDI threshold. Sooner or later, sufficiently far away from the PDI threshold, the SO process will take over. And it will mark the breakup of the PDI proportionality to $(e, 2e)$. In the inner atomic shells, the scaling of PDI to $(e, 2e)$ is extended sufficiently far because the pole approximation holds well for these inner-shell PDI processes. In addition, the first-order perturbative treatment of the electron-electron interaction displayed in Fig. 1 becomes more justifiable. In particular, in the He-like Mg^{10+} ion, this proportionality holds at photon energies up to 5 ionic ionization potentials. In the F^- ion, it is maintained up to $10I_p^+$. The asymptotic double-to-single ratio in this target

$\sigma_{\gamma^{2+}}/\sigma_{\gamma^+}|_{\omega \rightarrow \infty} \simeq 2\%$. This ratio is calculated via the overlaps of the atomic and ionic orbitals obtained with the GRASP code [24]. It is less than 10% of the peak value. So this limit and the onset of the SO process are reached well outside the experimentally accessible photon energy range. It is for this reason that the proportionality of the PDI to $(e, 2e)$ holds so well in the experiment [9].

More generally, $(e, 2e)$ calculations on many-electron targets are much less computationally demanding than PDI calculations. Hence a universal dynamic scaling of PDI to $(e, 2e)$ in inner atomic shells opens a wide avenue for theoretical interpretation of high photon energy experiments. These experiments now have become accessible with the advent of high-brightness x-ray synchrotron radiation sources [25] in combination with state-of-the-art experimental techniques [9].

ACKNOWLEDGMENTS

It gives the author a great pleasure to express his sincere gratitude to Prof. A. Müller for many stimulating discussions as well as for critical reading of the manuscript and the numerical data.

-
- [1] R. Wehlitz, *Simultaneous Emission of Multiple Electrons from Atoms and Molecules Using Synchrotron Radiation*, Advances in Atomic, Molecular, and Optical Physics Vol. 58 (Academic, New York, 2010), pp. 1–76.
- [2] J. H. McGuire, *Electron Correlation Dynamics in Atomic Collisions*, Cambridge Monographs on Atomic, Molecular and Chemical Physics (Cambridge University Press, Cambridge, 1997).
- [3] T. Schneider, P. L. Chocian, and J.-M. Rost, Separation and Identification of Dominant Mechanisms in Double Photoionization, *Phys. Rev. Lett.* **89**, 073002 (2002).
- [4] A. Knapp, A. Kheifets, I. Bray, T. Weber, A. L. Landers, S. Schössler, T. Jahnke, J. Nickles, S. Kammer, O. Jagutzki *et al.*, Mechanisms of Photo Double Ionization of Helium by 530 eV Photons, *Phys. Rev. Lett.* **89**, 033004 (2002).
- [5] J. Hozzowska, A. K. Kheifets, J.-C. Dousse, M. Berset, I. Bray, W. Cao, K. Fennane, Y. Kayser, M. Kavčič, J. Szlachetko *et al.*, Physical Mechanisms and Scaling Laws of K-Shell Double Photoionization, *Phys. Rev. Lett.* **102**, 073006 (2009).
- [6] J. A. R. Samson, Proportionality of Electron-Impact Ionization to Double Photoionization, *Phys. Rev. Lett.* **65**, 2861 (1990).
- [7] A. S. Kheifets, A. Ipatov, M. Arifin, and I. Bray, Double-photoionization calculations of the helium metastable $2^{1,3}S$ states, *Phys. Rev. A* **62**, 052724 (2000).
- [8] A. S. Kheifets, On different mechanisms of the two-electron atomic photoionization, *J. Phys. B* **34**, L247 (2001).
- [9] A. Müller, A. Borovik Jr, S. Bari, T. Buhr, K. Holste, M. Martins, A. Perry-Saßmannshausen, R. A. Phaneuf, S. Reinhardt, S. Ricz *et al.*, Near-K-Edge Double and Triple Detachment of the F^- Negative Ion: Observation of Direct Two-Electron Ejection by a Single Photon, *Phys. Rev. Lett.* **120**, 133202 (2018).
- [10] T. Andersen, Atomic negative ions: Structure, dynamics and collisions, *Phys. Rep.* **394**, 157 (2004).
- [11] T. Pattard, A shape function for single-photon multiple ionization cross sections, *J. Phys. B* **35**, L207 (2002).
- [12] A. S. Kheifets and I. Bray, Photoionization with excitation and double photoionization of helium isoelectronic sequence, *Phys. Rev. A* **58**, 4501 (1998).
- [13] A. S. Kheifets, D. V. Fursa, and I. Bray, Two-electron photoionization of ground-state lithium, *Phys. Rev. A* **80**, 063413 (2009).
- [14] M. I. Amusia and L. V. Chernysheva, *Computation of atomic processes: A handbook for the ATOM programs* (Institute of Physics, Bristol, 1997).
- [15] M. Y. Amusia, N. A. Cherepkov, L. V. Chernysheva, D. M. Davidović, and V. Radojević, Slow-electron elastic scattering on argon, *Phys. Rev. A* **25**, 219 (1982).
- [16] J. S. Bell and E. J. Squires, A Formal Optical Model, *Phys. Rev. Lett.* **3**, 96 (1959).
- [17] D. A. Varshalovich, A. N. Moskalev, and V. K. Khersonskii, *Quantum Theory of Angular Momentum*, 1st ed. (World Scientific, Philadelphia, 1988).
- [18] L. D. Landau and E. M. Lifshitz, *Quantum Mechanics (Non-Relativistic Theory)*, Course of Theoretical Physics Vol. 3, 3rd ed. (Pergamon, Oxford, 1985).
- [19] I. E. McCarthy and A. T. Stelbovics, Momentum-space coupled-channels optical method for electron-atom scattering, *Phys. Rev. A* **28**, 2693 (1983).
- [20] I. Bray, D. Fursa, A. Kadyrov, A. Stelbovics, A. Kheifets, and A. Mukhamedzhanov, Electron- and photon-impact atomic ionisation, *Phys. Rep.* **520**, 135 (2012).
- [21] A. Borovik, Jr., A. Müller, S. Schippers, I. Bray, and D. V. Fursa, Electron impact ionization of ground-state and metastable Li^+ ions, *J. Phys. B* **42**, 025203 (2009).
- [22] R. Dörner, T. Vogt, V. Mergel, H. Kheifets, S. Kravis, C. L. Cocke *et al.*, Ratio of Cross Sections for Double to Single

- Ionization of He by 85–400 eV Photons, [Phys. Rev. Lett.](#) **76**, 2654 (1996).
- [23] J. J. Yeh, *Atomic Calculation of Photoionization Cross-Sections and Asymmetry Parameters* (Gordon and Breach, Langhorne, PA, 1993).
- [24] K. G. Dyall, I. P. Grant, C. T. Johnson, F. P. Parpia, and E. P. Plummer, GRASP: A general-purpose relativistic atomic structure program, [Comput. Phys. Commun.](#) **55**, 425 (1989).
- [25] H. Franz, O. Leupold, R. Röhlberger, S. Roth, O. Seeck, J. Spengler, J. Stempfer, M. Tischer, J. Viefhaus, E. Weckert *et al.*, PETRA III: DESY's new high brilliance third generation synchrotron radiation source, [Synchrotron Radiat. News](#) **19**, 25 (2006).